Hematoxylin and Eosin Stained Histopathological Image Enhancement Method

Bogusław Cyganek AGH University of Krakow, Al. Mickiewicza 30, 30-059 Kraków, Poland

Keywords: Medical Image Processing, Histopathology, H&E Staining, Whole Slide Images (WSI),

High-Dynamic Range, Image Enhancement, Deep Learning.

Abstract: Hematoxylin and eosin staining is one of the most well-known and common methods of staining histopathological samples. Its main purpose is to highlight the morphological features of tissues, which help

histopathological samples. Its main purpose is to highlight the morphological features of tissues, which help doctors make the right diagnosis. However, it is not without its flaws, and the scans obtained in this way are characterized by high inconsistency not only resulting from the variability of the tissues themselves, but also due to the chemical reagents used, the technique of preparing the preparation, etc. This causes various difficulties and errors in the case of tissue assessment performed by the algorithm, but can also be a hindrance for doctors. Therefore, there are many methods to improve the quality of scans obtained from tissue stained in the H&E way. In this article, we present a fairly recent idea and very preliminary results for the use of our multi-channel virtual high-dynamic range MVHDR method to improve the parameters of H&E scans. Our method allows both data augmentation for CNN, but also significant detail enhancement that helps doctors

identify the disease.

1 INTRODUCTION

The examination of a tissue sample is one of the basic medical procedures in the diagnosis of various types of cancer in humans and animals. For this purpose, there are strict procedures for collecting such tissues and then properly preparing, storing and - recently digitizing them into so called Whole Slide Images (WSI) (Tellez 2019, Janowczyk 2019, Greeley 2024). One of the very important steps in this chain is the appropriate staining of the tissue. Hematoxylin and eosin stain (H&E) is one of the principal tissue stains used in histology for over a century (Tellez 2019).

Hematoxylin is a natural chemical compound obtained from the logwood tree *Hematoxylon campechianum*, discovered by the Spanish during exploration expeditions to Yucatan, Mexico, in the early 16th century. Hematoxylin's initial uses were for dyeing hair and fabrics. The first tissue staining with hematoxylin dates back to 1800. Interestingly, for over 200 years, hematoxylin has remained one of the primary methods of staining tissue, primarily for the isolation of nuclei in microscope slides (Titford 2005). Despite many years and the development of other methods, H&E is the most widely used stain in biology and medical diagnosis and is often the gold

standard (Dapson 2009)(Bassotti 2011)(Ma 2024). For example, when a pathologist looks at a biopsy of a suspected cancer, the histological section is likely to be H&E stained (Sorenson 2014)(Srinidhi 2021).

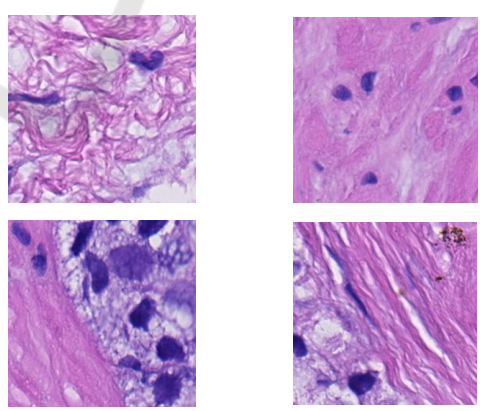


Figure 1: Examples of the healthy prostate tissue (upper row) and tissues with cancer of type Gleason 5 (lower row). Scans from the DiagSet dataset (Koziarski 2024).

Figure 1 shows patches extracted from a WSI scan of the DiagSet dataset containing examples of prostate tissues from the anonymous patients (Koziarski 2024). Upper row contains the healthy

prostate tissues, while the lower one shows patches with a prostate cancer classified by an expert to Gleason grade no. 5.

As already mentioned, H&E uses two histological stains – hematoxylin (H) and eosin (E). H affects cell nuclei and renders them purplish blue. On the other hand, E stains in pink mostly the extracellular matrix and cytoplasm, whereas other structures take on different shades, hues, as well as combinations of similar colors. A brief explanation of the main structures visible in a tissue sample after the H&E staining is shown in Figure 2 (Lisowski 2019) (Sampias 2025). Hence a pathologist can easily differentiate between the nuclear and cytoplasmic parts of a cell, and additionally, the overall patterns of coloration from the stain show the general layout and distribution of cells and provides a general overview of a tissue sample's structure. Thus, pattern recognition, both by expert humans themselves and by software that aids those experts in digital pathology, provides histologic information.

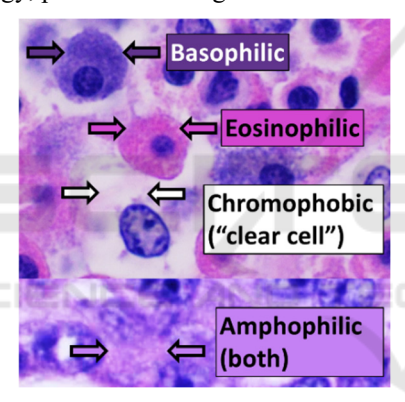


Figure 2: Brief explanation of the main structures visible in a tissue sample after the hematoxylin & eosin staining (Source images: Mikael Häggström. Public Domain, 2022).

Nevertheless, H&E is not a remedy for all the cases and tissues – hence, in some difficult cases more specific stains and methods are used. Similarly, when using H&E stained patches for grading we may encounter a number of problems. The first problem is the heterogeneity of samples even those performed in the same laboratory. The second is the insufficient quality parameters of the image that make it difficult or negatively affect the quality of classification.

In this paper we address at least two of these problems by proposing a new concept of nonlinear multi-channel virtual high dynamic range (MVHDR) filtering method, however successfully applied to the H&R scans. What's important about our method is that it follows the general idea of tissue staining – because unstained tissues lack contrast, our method

goes a step further and significantly improves contrast in already H&E stained tissues.

This our preliminary proof of concept is based on a number of previous works and discoveries that inspired us to use it to improve the quality of H&E scans based on the advance image filtering algorithms (Grabek 2019)(Koziarski 2018). These previous observations include the application of VHDR to thermal images, i.e. from the far infrared, for which we observed that the application of VHDR before using the CNN network significantly improved its results (Knapik 2019). Early concepts and results, presented in this paper, show that our assumptions are correct, although we leave more in-depth studies for the future

This is a position paper showing our initial concepts and the first observations. The rest of the paper is organized as follows. In Section 2, we briefly review the existing literature on this topic. In Section 3, we present the details of our approach, with a novel multi-channel VHDR (MVHDR). Chapter 4 presents the results of the experiments along with a discussion of the obtained results. The article ends with conclusions and a list of literature.

2 RELATED WORKS

The history of the discovery of hematoxylin, as well as its subsequent uses, is particularly interesting (Titford 2005)(Cooksey 2021). Despite numerous studies and new approaches to tissue contrast, H&E remains one of the most widely used methods. However, it is not without its drawbacks (Dapson 2009)(Bassotti 2011)(Ma 2024). Hence, there are many works and studies on improving the image quality of scans stained in the H&E method. Here we mention only a few of the most important ones, and further literature references can be found in the mentioned here works. The first group are methods improving the repeatability and homogenity of staining, because even the same laboratories can produce completely different shades for the same tissues. These are called stain normalization methods. In this respect Janowczyk et al. proposed the use of sparse autoencoders for stain normalization (Janowczyk 2017). In their method pixels are separated into k clusters. Then histogram equalization across clusters and RGB channels is applied to obtain a color standardized image. In the same vein Zanjani et al. propose to use the deep generative models (Zanjani 2018). This is done to separate pixels into ktissue classes. In the next step, stain normalization is obtained by separation of the source and target

images. On the other hand, for stain normalization Tellez et al. propose an U-Net-like network architecture. This is improved with heavily color-augmented images and trained to reconstruct their original appearance (Tellez 2019). Their main idea is that when trained with images from a target center, the network should be able to transform new images to the same target color distribution.

The second group of methods deals with the general change of parameters of H&E images. An interesting approach is based on Blind Color Deconvolution (BCD) techniques. Its idea is to separate H&E images into colors (stains) and structural information (concentrations). This, in turn, can be useful for the further processing, data augmentation, and classification etc. In this respect, Ruifrok et al. proposed the use of the logarithmically inverted optical density space and a non-blind color deconvolution algorithm to obtain the stain concentrations (Ruifrok 2001).

However, we have adopted a slightly different approach, which involves both improving contrast and the ability to change the color space.

3 METHOD DESCRIPTION

In this section the basic architecture of the proposed method is presented. More concretely, we start with the overall view of the main blocs, after which a general description of the method operation follows.

3.1 Operation of the Virtual High-Dynamic Range Converter

The main idea of the presented method, called VHDR (Knapik 2021), is to increase the dynamics of the image, but using a single image as its input – hence the name "virtual" high dynamic range. This is different from classic HDR, which usually uses several images with different exposures (Sen 2016). However, in many cases, such as H&E, we simply do not have such many exposures. Hence the idea that we can "artificially" generate them. The processing chain leading to this is shown in Figure 3. It operates as follows. An input image is processed by a set of tone adjustment curves. As a result, a number of tone converted images is calculated.

The main idea here is to expose different ranges of the input image, in order to reveal not well visible details. The tone sub-images are then joined back to form one HDR image. After that, image range conversion and contrast enhancement are applied.

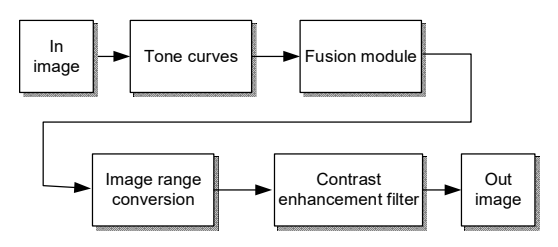


Figure 3: Architecture of the virtual high-dynamic range converter. Only a single image is required as its input.

The luminance change is done with help of the logistic function, in its basic form given as follows

$$s_0(x) = A/(1 + e^{-k(x-x_0)}),$$
 (2)

where A denotes and amplitude and k is a parameter; x_0 denotes the so called middle point of the S shape function, whose inflection point is just x_0 .

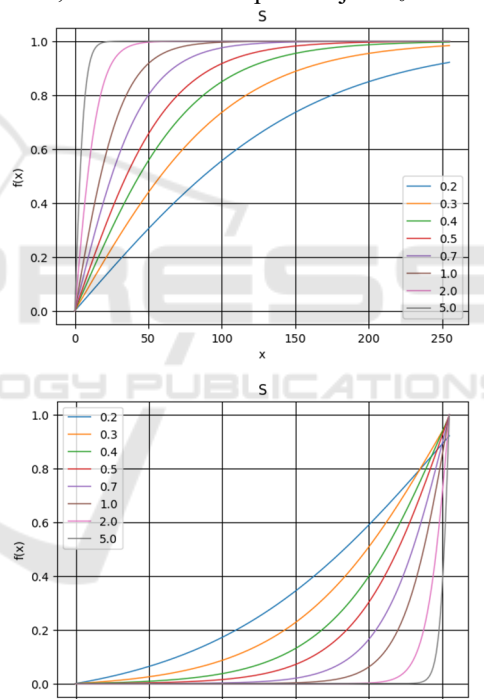


Figure 4: Sets of functions to generate virtual exposures. Horizontal axis denotes the input brightness. Vertical the normalized output brightness. From top: convex and concave curves.

150

However, to generate series of virtual exposures we need three variants of the logistic functions: convex, concave, as well as S-shaped. Exemplary variants of these function are shown in Figure. Not less important is to assure that the domain and codomain cover the whole allowable range, which for

8-bits runs 256 values. Hence (1) needs to be conditioned, as follows

$$s_1(x,k,x_0) = A/1 + e^{-Dk\frac{(x-x_0)}{R}}$$
 (2)

D is a domain range constant, $A=P_{max}$ is a maximal pixel range of the input image. The parameter D controls the range of values of s_1 – it needs to be different from 0 and 1. In other words, these are the saturation values. In our system this parameter is set to 2 times 6 around x_0 , and hence D=12.

The above function is extended by the additional multiplicative and additive components to provide a concave, convex and S like shape. It needs also to cover full range of the codomain – this is in the range $[P_{min}, P_{max}]$, i.e. [0,255]. Hence, new version of () reads as follows:

$$s_{2}(x,k,x_{0}) = s_{1}(x,k,x_{0})(|x_{0} - P_{mid}|/P_{mid} + 1) + s_{1}(0,k,x_{0})$$
(3)

For 8-bit pixel representations P_{mid} =(P_{max} - P_{min})/2=(255.0-0.0)/2=127.5, which denotes a middle value of the low dynamic image. In the next step, parameter x_0 is chosen from the following three values

$$x_0 \in \left\{ P_{min}, P_{mid}, P_{max} \right\}. \tag{4}$$

Each of the above values of x_0 corresponds to a distinct type of a curve as follows (Figure 4):

- 1. Convex case The midtone data of the input image is stretched toward the highlight of the output space, resulting in a bright-toned image.
- 2. Concave case The midtone data of the input is stretched toward the shadow of the output space, resulting in a dark-toned image.
- 3. S-curve The highlight and shadow of the input pixels are enhanced, leading to a higher contrast.

The parameter to consider now is k, whose value was chosen experimentally, as follows:

$$k \in \begin{cases} \{0.2, 0.3\}, for \, x_0 = P_{min} \\ \{0.4, 0.5\}, for \, x_0 = P_{mid} \\ \{0.3, 0.4\}, for \, x_0 = P_{max}. \end{cases}$$
 (5)

Summarizing, with three values x_0 , and two parameters k for each x_0 , a series of V=6 tone converted images I_v is generated. Values of these parameters were chosen experimentally.

On the other hand, the fusion module takes as its input the aforementioned set of V tone mapped images. In its next step, each pixel i_h in the output fused image I_h is computed as a weighted sum of all V pixels i_v , as follows

$$i_h = \sum_{v=1}^{V} w_v i_v / \sum_{v=1}^{V} w_v , \qquad (6)$$

where i_h denotes an output pixel, i_v is an input pixel from one of the V tone mapped images I_v , while the weight w_v is computed as follows:

$$w_{i,} = e^{-\lambda \left(\frac{i_{v} - P_{mid}}{P_{mid}}\right)^{2}}.$$
 (7)

 λ in the above denotes a parameter that controls steepness of the weighting function. In our experiments λ is set to a value in the range 2.2-3.9.

Pixel values obtained thanks to (6) are frequently concentrated around the middle values of the allowable pixel range, since these are increased by the weights in (7). Therefore, their values need to be further scaled by the image range conversion module, in order to spread equally their histograms. This scaling process is done as follows:

$$\hat{i}_h = \frac{i_h - min(I_h)}{max(I_h) - min(I_h)} P_{\text{max}}, \text{ for each } i_h \in I_h$$
 (8)

where $min(I_h)$ and $max(I_h)$ are minimal and maximal values of the whole I_h image, respectively.

The last step constitutes image contrast enhancement. This is done with the one-scale local spatial filter (Cvetkovic, 2007). In this process, each pixel is converted as follows:

$$i_o = \hat{i}_h + \left[\hat{i}_h - m(\hat{i}_h)\right],\tag{9}$$

where the mean value m around a pixel \hat{i}_h , in the window controlled by two parameters s_w and t_w , is computed in accordance with the following formula

$$m(\hat{i}_{h}(p,q)) = \frac{1}{(2s_{w}+1)(2t_{w}+1)} \sum_{s=-s_{w}}^{s_{w}} \sum_{t=-t_{w}}^{t_{w}} \hat{i}_{h}(p+s,q+t).$$
(10)

Figure 4 shows different functions for generation of virtual exposures.

3.2 Multi-Channel VHDR

The VHDR method described in the previous chapter has been extended to the space of color images or even multi-channel signals/images. This is one of the main contributions of this paper.

We assume that the input color image is represented using the RGB space. Then, an optional conversion of this space to another color space takes place. Out tested transformations are as follows:

- 1. RGB → HSI
- 2. RGB → IJK
- 3. RGB → YCrCb

In each of the above spaces, including RGB, the image dynamics improvement is performed independently in each of the color channels. This means that it is possible to independently select the parameters of the single-channel VHDR method for each color channel independently. In this way, for example, after transformation to the YCrCb space, only the Y channel can be modified, leaving Cr and Cb unchanged, etc. Operation of the proposed extended method is depicted in Figure 5.

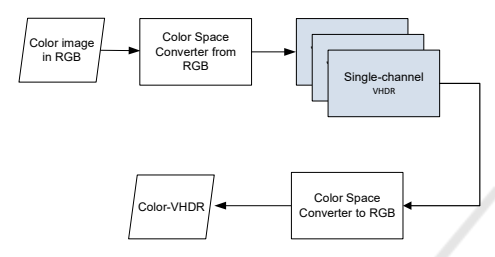


Figure 5: Architecture of the proposed multi-channel VHDR method. Structure of the single-channel VHDR is shown in Figure 3.

It is also possible to change all channels, also causing a change in the color palette. The last feature can be independently useful for doctors for deeper analysis of histopathological scans. Selected experimental results are presented in the next section.

4 EXPERIMENTAL RESULTS

As alluded to previously, in this position paper we present our novel concept and intuition, as well as initial findings. Our method is also underpinned with good results obtained in thermal image enhancement when operating with CNN (Knapik 2021). The main experiment planned for the nearest future research into this topic will be to train CNN for cancer classification with MVHDR on its input. This requires finding the optimal hyperparameters of MVHDR. Hence, the next step can be to built-in MVHDR as an initial layer of a CNN, which will be then trained with the optimization criteria of the best accuracy. However, this is left for the future research.

An interesting and parallel branch of method assessment is its application in computer systems aimed at helping to diagnose or to annotate WSI by the professional pathologists. Based on our private conversations with the pathologists we know their needs. We can also assess the usefulness of such

system features as the increase in scan quality presented here or the change of the color palette for the histopathological diagnostic process. It will therefore be a human-in-the-loop system.

Following this direction, in this paper we present results comparing the quality of patches from WSI scans before and after applying MVHDR. Our objective measures are sharpness and clarity.

• Sharpness – a measure conveying information on level of detail in a scan. In our approach we compute variance of the Laplacian, defined as follows (Cyganek 2009):

$$L[I(x,y)] = \nabla^2 I(x,y) = \frac{\partial^2 I}{\partial x^2} + \frac{\partial^2 I}{\partial y^2}, \quad (11)$$

In our experiments a discrete version of L is used, to compute sharpness coefficient S over an image I, as follows:

$$S[\mathbf{I}] = \operatorname{var}\left[\tilde{L}(\mathbf{I})\right],$$
 (12)

where $\tilde{L}(\mathbf{I})$ denotes discrete Laplacian over the entire image I, and var stands for variance. Hence, this measure indicates how well the edges and fine details are captured. In many classification systems, also based on AI, sharpness can be essential to obtain high accuracy especially when processing images with some lighting and/or geometrical defects.

Clarity – a measure that encompasses the overall visual coherence and an overall level of noise and/or distortions. In our approach clarity C is expressed as a product of the above sharpness measure S, and the standard deviation of an image. Hence, clarity is expressed as follows:

$$C[\mathbf{I}] = S[\mathbf{I}] \cdot std[\mathbf{I}], \tag{13}$$

where std is the standard deviation.

Figure 6 shows a number of original H&E patches from the DiagSet with various Gleason degrees (Koziarski 2024), i.e. these are cancerous tissues.

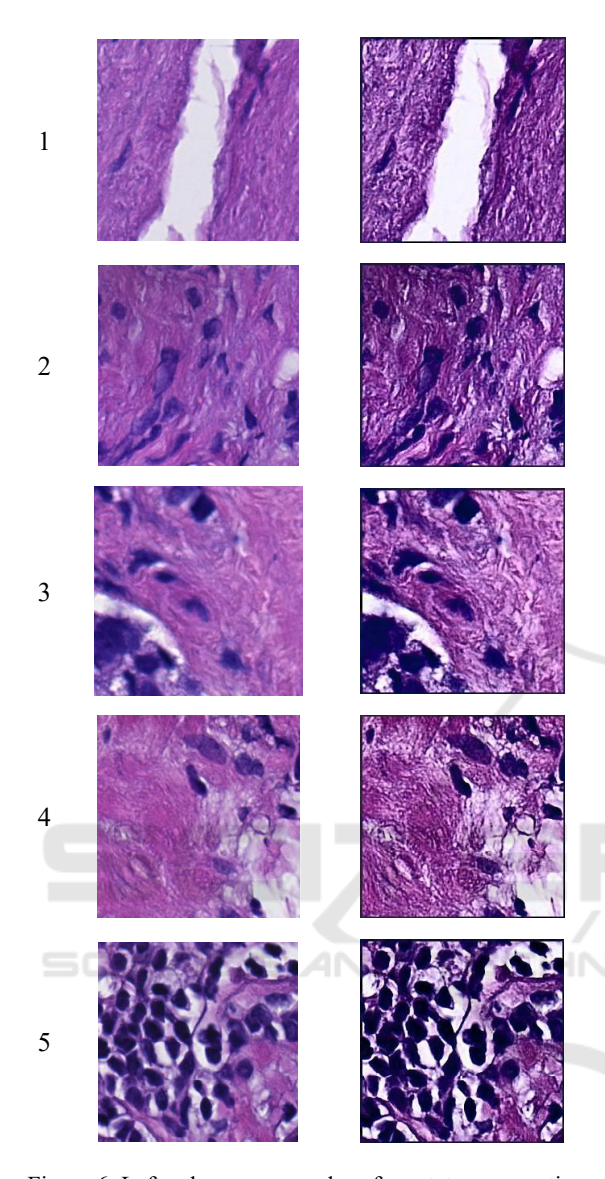


Figure 6: Left column – examples of prostate scan sections at 40x magnification from DiagSet – diseased tissue – G5 on the Gleason scale. Right column – images processed with the developed MVHDR module. Visible improvement in contrast enabling analysis of morphological structures of the tissue, such as estimation of the size and locations of nucleoli.

In Figure 6 original patches are in the left column, whereas MVHDR processed in the right one. Even visual inspection shows that the latter are sharper and more revealing of the morphological details of the tissue, which may be important both for classification, as well as for inspection by an expert pathologist. These observations are confirmed by quantitative measurements of the parameters S from (12) and C defined in (13), and presented in Table 1 and Table 2, respectively.

Table 1: Sharpness values S computed for the images from Figure 6.

Image no.	S - Original	S - MVHDR	Ratio
1	148.27	2465.83	16.6
2	155.66	2398.71	15,4
3	108.11	1690.45	15,6
4	219.39	3246.61	14,8
5	288.54	3376.86	11,7

Figure 7 shows prostate cancer tissues showing color space change obtained on histopathological scans using the developed MVHDR method. Original H&E patches are shown in the left column, while MVHDR-processed image are in the right one.

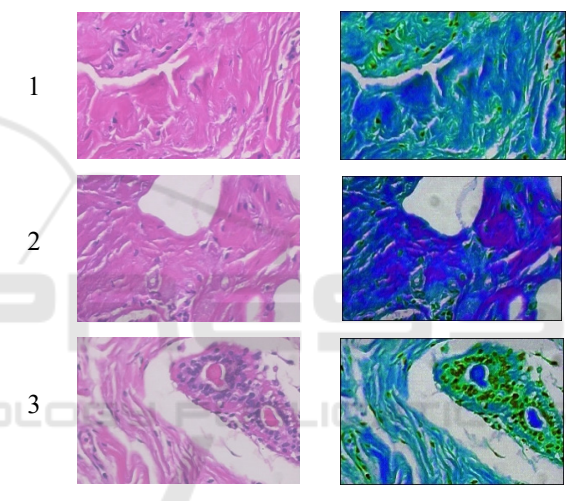


Figure 7: Samples of the prostate cancer tissues illustrating image enhancement and color space change by the MVHDR method. Original H&E image (left column), MVHDR-processed image (right column).

As can be seen in the right column of Figure 7, the histological images have not only been contrast-enhanced, but also converted to a different color space, which allows for the perception of other image details, e.g., in the case of a diagnosis made by a pathologist.

Table 2: Clarity values C computed for the images from Figure 6.

Image no.	C- Original	C - MVHDR	Ratio
1	6957.79	184386.41	26.5
2	4143.99	128363.72	30.9
3	4065.20	104402.24	25.7
4	8071.64	212568.42	26.3
5	16212.25	281219.42	17.3

Table 3 and Table 4 show numerical results of the parameters S and C computed for the images from Figure 7, respectively.

Table 3: Sharpness values S computed for the images from Figure 7.

Image no.	S - Original	S - MVHDR	Ratio
1	597.25	4647.94	7.8
2	301.59	3412.69	11.3
3	288.05	3777.61	13.1

Table 4: Clarity values C computed for the images from Figure 7.

Image no.	C- Original	C - MVHDR	Ratio
1	12583.80	188048.80	14.9
2	8096.60	188842.25	23.3
3	8106.07	189127.10	23.3

In all cases we see a significant difference, i.e. more than an order of magnitude, between the parameters for the original H&E scans and their versions processed with our MVHDR method. However, it's not the numerical values themselves that matter, but their ratio (the rightmost column), which in all cases exceeds an order of magnitude. This demonstrates significant potential for improving contrast, as well as the dynamics of pixel representation itself. We have presented results here for several images, but they are consistent for all patches obtained from the WSI scan. This proves the stability of the proposed method, which in virtually every real case leads to a significant contrast enhancement and – as we have seen – also allows for changing the color palette.

The presented method was implemented in C++. Experiments were conducted on a computer with 128 GB of RAM and an Intel® i7-11850H/2.50GHz microprocessor, running Windows 10 Pro. Such implementation allows for real-time processing of video streams, as well as for easy parallelization – the feature which we intend to utilize in the future.

5 CONCLUSIONS

In this paper we address the problem of enhancement and filtering of the H&E stained histopathological scans. Our original concept relies on application of the nonlinear multi-channel virtual high dynamic range filtering method to the H&R scans.

We would like to stress that this is an initial concept describing work in progress and published as a position paper. Therefore we only outlined the main concept and presented the initial results, which are encouraging. Also, our previous experience with this type of data preprocessing/augmentation for CNN training, although tested for thermal images showed very good results, increasing the final accuracy by certain percentage points (Knapik 2021).

Summarizing, our proposed MVHDR method can be used for:

- Data augmentation for CNN/ViT training.
- Generation of new images for GAN.
- To generate better quality histopathological images for doctors' diagnosis.

Our scientific hypothesis and things to do are as follows:

- 1. The proposed method, when used as a data preprocessing module, can lead to higher accuracies in deep learning with CNN and ViT.
- 2. The proposed method can be used as a data augmentation module.
- 3. The method can be used to improve quality and/or change the color palette when used in tissue diagnosis by medical experts.

If the above are correct, then the next step would be as follows:

4. Design of the input layers, so the optimal parameters of the MVHDR method can be learned by a CNN/ViT during its training.

Finally, we would like to mention that this method was discussed and pre-tested by two pathology experts who gave it a positive review. They were particularly interested in the possibility of enhancing the contrast and highlighting important morphological details of the observed tissues. We are planning further tests in this direction as well. It would be particularly interesting to observe differences in the labeling process of different types of tissue by medical specialists without and with the use of the method proposed here.

ACKNOWLEDGMENT

Research under project no. 10741, supported by program "Excellence initiative – research university" for the AGH University of Krakow.

REFERENCES

- Bassotti, G., Villanacci, V., Salerni, B., Maurer, C. A., Cathoma, G. (2011). Beyond hematoxylin and eosin: the importance of immunohistochemical techniques for evaluating surgically resected constipated patients Tech. Coloproctol 15:371–375, Springer, DOI 10.1007/s10151-011-0721-5.
- Cooksey, C. J. (2021) Hematoxylin in the 21st century, Biotechnic & Histochemistry, 96:3, pp. 242-249, DOI: 10.1080/10520295.2020.1786725
- Cvetkovic S.D., Schirris J., de With P.H.N. (2007). Locally-Adaptive Image Contrast Enhancement without Noise and Ringing Artifacts. IEEE International Conference on Image Processing, vol. 3, pp. 551-560.
- Cyganek, B. (2009). An Introduction to 3D Computer Vision Techniques and Algorithms, Wiley,.
- Dapson RW., Horobin RW. (2009). Dyes from a twenty-first century perspective, Biotechnic & Histochemistry, 84:4, pp. 135-137, DOI: 10.1080/10520290902908802
- Dosovitskiy, A., Beyer, L., Kolesnikov, A., Weissenborn,
 D., Zhai, X., Unterthiner, T., Dehghani, M., Minderer,
 M., Heigold, G., Gelly, S. (2020). An image is worth
 16x16 words: Transformers for image recognition at
 scale. arXiv preprint. arXiv: 2010.11929.
 https://doi.org/10.48550/arXiv.2010.11929.
- Grabek, J., Cyganek, B (2019). Speckle Noise Filtering in Side-Scan Sonar Images Based on the Tucker Tensor Decomposition, Sensors, 19(13), 2903; https://doi.org/ 10.3390/s19132903
- Greeley, C., Holder, L., Nilsson, E. E., Skinner, M. K. (2024). Scalable deep learning artificial intelligence histopathology slide analysis and validation. Scientific Reports, 14(1), 26748. https://doi.org/10.1038/s41598-024-76807-x.
- Janowczyk A, Madabhushi A. (2016). Deep learning for digital pathology image analysis: a comprehensive tutorial with selected use cases. J Pathol Inform;7(1):29.
- Janowczyk, Basavanhally, A., Madabhushi A. (2017). Stain normalization using sparse autoencoders (stanosa): application to digital pathology, Comput. Med. Imaging Graph. 57.
- Ke W.-M., Wang T.-H., Chiu C.-T. (2009). Hardware-efficient virtual high dynamic range image reproduction. Proceedings of the 16th IEEE International Conference on Image Processing (ICIP'09). Piscataway, NJ, USA: IEEE Press, pp. 2665–2668.
- Knapik M., Cyganek B. (2021). Fast eyes detection in thermal images. Multimedia Tools and Applications 80:3601–3621, Springer, https://doi.org/10.1007/ s11042-020-09403-6.
- Koziarski, M., Cyganek, B. (2018). Marine Snow Removal Using a Fully Convolutional 3D Neural Network Combined with an Adaptive Median Filter, 24th International Conference on Pattern Recognition,

- Pattern Recognition And Information Forensics (ICPR 2018) LNIP Vol. 11188, pp. 16-25
- Koziarski, M., Cyganek, B., Niedziela, P., Olborski, B., Antosz, Z., Żydak, M., Kwolek, B., Wąsowicz, P., Bukała, A., Swadźba, J. (2024). DiagSet: A dataset for prostate cancer histopathological image classification. Scientific Reports, 14(1), 6780. Nature Publishing Group. https://doi.org/10.1038/s41598-024-52183-4.
- Lisowski, A. (2019) Science of H&E. Leica BioSystems https://www.leicabiosystems.com/knowledge-pathway/science-of-he/
- Ma, ZY, Zhang, XF, Hu, YZ, Zhu, MD, Jin, J, Qian, P. (2024). Comparison of staining quality between rapid and routine hematoxylin and eosin staining of frozen breast tissue sections: an observational study. J Int Med Res. Jun; 52(6): 3000605241259682. doi: 10.1177/03000605241259682. PMID: 38886869; PMCID: PMC11184997.
- Ruifrok A.C., Johnston D.A. (2001). Quantification of histochemical staining by color deconvolution, Anal. Quant. Cytol. Histol. 23, pp. 291–299.
- Sampias, C., Rolls, G. (2025). H&E Staining Overview: A Guide to Best Practices. Leica BioSystems. https://www.leicabiosystems.com/knowledge-pathway/he-staining-overview-a-guide-to-best-practices/
- Sen P., Aguerrebere C. (2016). Practical High Dynamic Range Imaging of Everyday Scenes. IEEE Signal Processing Magazine, pp. 36-44.
- Srinidhi, C.L., Ciga, O., Martel, A.L. (2021). Deep neural network models for computational histopathology: A survey, Medical Image Analysis, Volume 67, 2021, 101813, ISSN 1361-8415, https://doi.org/10.1016/j. media.2020.101813.
- Sorenson, R.L., Brelje, T.C. (2014). Atlas of Human Histology A Guide to Microscopic Structure of Cells, Tissues and Organs 3rd Edition
- Tellez D, Litjens G, Bándi P. (2019). Quantifying the Effects of Data Augmentation and Stain Color Normalization in Convolutional Neural Networks for Computational Pathology Medical Image Analysis, Volume 58.
- Titford, M. (2005). The long history of hematoxylin, Biotechnic & Histochemistry, 80:2, pp. 73-78, Taylor & Francis.
- Zanjani F.G., Zinger S., Bejnordi, B.E., van der Laak, J.A., de With, P.H. (2018). Stain normalization of histopathology images using generative adversarial networks, in: 2018 IEEE 15th International Symposium on Biomedical Imaging, pp. 573–577, IEEE.